Displays 31 (2010) 191–195

Contents lists available at ScienceDirect

Displays

journal homepage: www.elsevier.com/locate/displa

An alternative bend-testing technique for a flexible indium tin oxide film

Yen-Liang Chen [a,b], Hung-Chih Hsieh [a], Wang-Tsung Wu [a], Bor-Jiunn Wen [b], Wei-Yao Chang [a], Der-Chin Su [a,*]

[a] Department of Photonics and Institute of Electro-Optical Engineering, National Chiao Tung University, 1001 Ta-Hsueh Road, Hsinchu 30010, Taiwan
[b] Center for Measurement Standards/Industrial Technology Research Institute (ITRI), Bldg. 16, 321, Kuang Fu Rd. Sec. 2, Hsinchu 30011, Taiwan

ARTICLE INFO

Article history:
Received 28 January 2010
Received in revised form 12 July 2010
Accepted 21 July 2010
Available online 24 July 2010

Keywords:
Indium tin oxide film
Bending test
Refractive index
Electro-optic modulation
Heterodyne interferometry

ABSTRACT

The two-dimensional refractive index distribution of a flexible indium tin oxide film deposited on a PET layer is measured before/after the bend-testing with an alternative technique based on Fresnel equations and the heterodyne interferometry. Their standard deviations are derived and they vary more obviously than the resistance variations measured in the conventional method. Hence the standard deviation of the refractive index can be used as the indicator to justify the durability of a flexible indium tin oxide film. The validity is demonstrated.

1. Introduction

Due to the high optical transmittance and the high conductivity of an indium tin oxide (ITO) film, it is widely used as the electrode for flat panel display devices, solar sells and organic light emitting diodes (OLED) [1]. In practice, the electronic patterns are printed on a thin ITO film deposited on a polyethylene terephthalate (PET) layer with laser patterning processes [2] to fabricate a flexible electronic substrate. The residual stress in part areas on the film caused by the temperature variation during the processes affects its quality and lifetime. The bending test can make the effect of the residual stress to be more obvious [3–7], so the resistance variation after definite bending cycles is always used as an indicator to justify its durability. However the resistance measurement is less sensitivity and the durability test becomes tedious due to its time-consuming bending cycles. To improve the sensitivity of this test, the two-dimensional microscopic refractive index distribution variations are observed instead of the conventional single-value resistance measurement.

Due to its photoelasticity [8], its refractive index is related with the residual stress. An alternative technique for measuring the two-dimensional refractive index distribution is presented based on Fresnel equations and the heterodyne interferometry. In this method, a collimated linearly/circularly polarized heterodyne light beam in turn enters a modified Twyman-Green interferometer, in which an ITO film is located in one arm for test. Two groups of full-field interference signals are taken by a fast CMOS camera. The sampling intensities recorded at each pixel are fitted to derive a sinusoidal signal, and its associated phase can be calculated. Then, substituting these two groups of phase distribution data into the special equations derived from Fresnel equations, its two-dimensional refractive index distribution and the standard deviation can be estimated. This film is tested before/after some different bending cycles. The standard deviation varies more obviously than the resistance variation measured with the conventional method. Hence the standard deviation of the two-dimensional refractive index distribution can be used as an indicator to justify its durability. The validity of this technique is demonstrated.

2. Principle

Fig. 1 shows a schematic diagram of this technique. For convenience, the $+z$-axis is chosen to be along the light propagation direction and the $+y$-axis is along the direction pointing out the paper plane. A light beam coming from a heterodyne light source [9] has a frequency difference f between the x- and the y-polarizations, and its Jones vector can be written as [10]

$$E_1 = \frac{1}{\sqrt{2}}\begin{pmatrix} e^{i\pi ft} \\ e^{-i\pi ft} \end{pmatrix}. \quad (1)$$

The light beam is expanded and collimated by a beam expander BE. It enters a modified Twyman-Green interferometer, which consists of a beam-splitter BS, a quarter-wave plates Q_2 with the fast axis at 45° with respect to the y-axis, a reference mirror M, a test sample S, an analyzer AN with the transmission axis at 0° with

* Corresponding author.
E-mail address: t7503@faculty.nctu.edu.tw (D.-C. Su).

0141-9382/$ - see front matter © 2010 Elsevier B.V. All rights reserved.
doi:10.1016/j.displa.2010.07.003

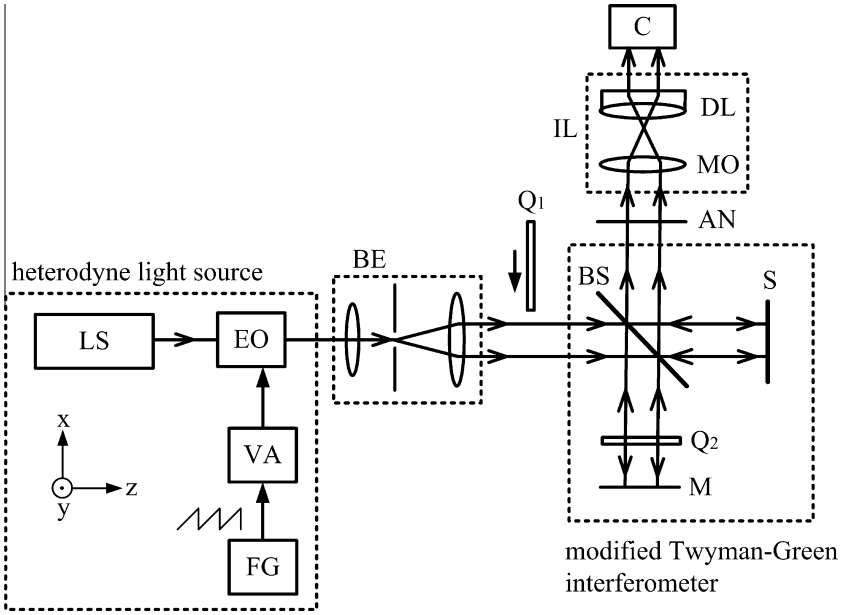

Fig. 1. Schematic diagram of this technique. LS: laser light source; EO: electro-optic modulator; FG: function generator; VA: voltage linear amplifier; BE: beam expander; Q: quarter-wave plate; BS: beam-splitter; M: mirror; S: sample; AN: analyzer; IL: imaging lens; MO: microscopic objective; DL: doublet; C: CMOS camera.

respect to the *y*-axis, an imaging lens IL, and a CMOS camera C. In this interferometer, two optical paths are (1) BS → Q_2 → M → Q_2 → BS → AN → IL → C (the reference beam), and (2) BS → S → BS → AN → IL → C (the test beam). For convenience, we firstly assume that the S is an isotropic material. So, their amplitudes can be derived and expressed as

$$\begin{aligned} E_{r1} &= (\mathrm{AN}(0^\circ)\cdot \mathrm{R_{BS}}\cdot \mathrm{Q}_2(-45^\circ)\cdot \mathrm{M}\cdot Q_2(45^\circ)\cdot E_1)\cdot e^{i\phi_{d1}} \\ &= \begin{pmatrix}1&0\\0&0\end{pmatrix}\begin{pmatrix}e^{-i\phi_r/2}&0\\0&e^{i\phi_r/2}\end{pmatrix}\frac{1}{\sqrt{2}}\begin{pmatrix}1&i\\i&1\end{pmatrix}\begin{pmatrix}-r_m&0\\0&r_m\end{pmatrix} \\ &\quad\times\frac{1}{\sqrt{2}}\begin{pmatrix}1&-i\\-i&1\end{pmatrix}\frac{1}{\sqrt{2}}\begin{pmatrix}e^{i\pi ft}\\e^{-i\pi ft}\end{pmatrix}e^{i\phi_{d1}} = \frac{ir_m e^{i(\phi_{d1}-\pi ft-\phi_r/2)}}{\sqrt{2}}\begin{pmatrix}1\\0\end{pmatrix}, \end{aligned} \tag{2}$$

and

$$\begin{aligned} E_{t1} &= (\mathrm{AN}(0^\circ)\cdot \mathrm{S}\cdot \mathrm{R_{BS}}\cdot E_1)\cdot e^{i\phi_{d2}} \\ &= \begin{pmatrix}1&0\\0&0\end{pmatrix}\begin{pmatrix}-r&0\\0&r\end{pmatrix}\begin{pmatrix}e^{-i\phi_r/2}&0\\0&e^{i\phi_r/2}\end{pmatrix}\frac{1}{\sqrt{2}}\begin{pmatrix}e^{i\pi ft}\\e^{-i\pi ft}\end{pmatrix}e^{i\phi_{d2}} \\ &= -\frac{re^{i(\pi ft+\phi_{d2}-\phi_r/2)}}{\sqrt{2}}\begin{pmatrix}1\\0\end{pmatrix}. \end{aligned} \tag{3}$$

Here, R_{BS}, M and S are the reflection matrix of the BS, M and S; r_m and r are the reflection coefficients of the M and the S; ϕ_{d1} and ϕ_{d2} are the phase variations due to the optical path lengths of the reference and test beam, respectively. ϕ_r is the phase difference between the *x*- and *y*-polarizations coming from the reflection at BS. Thus, the interference signals recorded by the C can be written as

$$\begin{aligned} I_A &= |E_{r1}+E_{t1}|^2 = I_{01}+\gamma_1\cdot\cos(2\pi ft+\phi_1) \\ &= \frac{1}{2}\{r^2+r_m^2-2rr_m\cos[2\pi ft+\frac{\pi}{2}-(\phi_{d1}-\phi_{d2})]\}, \end{aligned} \tag{4}$$

where I_{01}, and γ_1 and ϕ_1 are the mean intensity, the visibility and the phase of the interference signal, respectively. From Eq. (4), we have

$$\phi_1 = \frac{\pi}{2}-(\phi_{d1}-\phi_{d2}). \tag{5}$$

Secondly, the quarter-wave plate Q_1 with the fast axis at 45° to the *y*-axis is inserted into the optical setup as shown in Fig. 1 and the light amplitude becomes

$$\begin{aligned} E_2 &= \mathrm{Q}_1(45^\circ)\cdot E_1 = \frac{1}{2}\begin{pmatrix}1&-i\\-i&1\end{pmatrix}\begin{pmatrix}e^{i\pi ft}\\e^{-i\pi ft}\end{pmatrix} \\ &= \frac{1-i}{2}\begin{pmatrix}\cos(\pi ft)-\sin(\pi ft)\\\cos(\pi ft)+\sin(\pi ft)\end{pmatrix} = \frac{1}{2}\begin{pmatrix}1\\-i\end{pmatrix}e^{i\pi ft}+\frac{1}{2}\begin{pmatrix}-i\\1\end{pmatrix}e^{-i\pi ft}. \end{aligned} \tag{6}$$

From Eq. (6), we can see that there is a frequency difference *f* between the right- and the left-circular polarizations, and it is a circularly polarized heterodyne light beam.

The amplitudes of the reference beam and the test beam can be derived as above and expressed as

$$\begin{aligned} E_{r2} &= (\mathrm{AN}(0^\circ)\cdot \mathrm{R_{BS}}\cdot \mathrm{Q}_2(-45^\circ)\cdot \mathrm{M}\cdot \mathrm{Q}_2(45^\circ)\cdot E_2)\cdot e^{i\phi_{d1}} \\ &= \begin{pmatrix}1&0\\0&0\end{pmatrix}\begin{pmatrix}e^{-i\phi_r/2}&0\\0&e^{i\phi_r/2}\end{pmatrix}\frac{1}{\sqrt{2}}\begin{pmatrix}1&i\\i&1\end{pmatrix}\begin{pmatrix}-r_m&0\\0&r_m\end{pmatrix} \\ &\quad\times\frac{1}{\sqrt{2}}\begin{pmatrix}1&-i\\-i&1\end{pmatrix}\frac{1-i}{2}\begin{pmatrix}\cos(\pi ft)-\sin(\pi ft)\\\cos(\pi ft)+\sin(\pi ft)\end{pmatrix}e^{i\phi_{d1}} \\ &= \frac{i+1}{2}r_m[\cos(\pi ft)+\sin(\pi ft)]e^{i(\phi_{d1}-\phi_r/2)}\begin{pmatrix}1\\0\end{pmatrix}, \end{aligned} \tag{7}$$

and

$$\begin{aligned} E_{t2} &= (\mathrm{AN}(0^\circ)\cdot \mathrm{S}\cdot \mathrm{R_{BS}}\cdot E_2)\cdot e^{i\phi_{d2}} \\ &= \begin{pmatrix}1&0\\0&0\end{pmatrix}\begin{pmatrix}-r&0\\0&r\end{pmatrix}\begin{pmatrix}e^{-i\phi_r/2}&0\\0&e^{i\phi_r/2}\end{pmatrix}\frac{1-i}{2}\begin{pmatrix}\cos(\pi ft)-\sin(\pi ft)\\\cos(\pi ft)+\sin(\pi ft)\end{pmatrix}e^{i\phi_{d2}} \\ &= \frac{i-1}{2}r[\cos(\pi ft)-\sin(\pi ft)]e^{i(\phi_{d2}-\phi_r/2)}\begin{pmatrix}1\\0\end{pmatrix}. \end{aligned} \tag{8}$$

Here the interference signals measured by the *C* can be written as

$$\begin{aligned} I_B &= |E_{r2}+E_{t2}|^2 = I_{02}+\gamma_2\cdot\cos(2\pi ft+\phi_2) \\ &= A\cdot\cos(2\pi ft)+B\cdot\sin(2\pi ft)+C, \end{aligned} \tag{9}$$

where I_{02}, γ_2 and ϕ_2 are the mean intensity, the visibility and the phase of the interference signals, respectively. A, B, and C are real numbers. Here we have

$$A = rr_m \sin(\phi_{d1} - \phi_{d2}) \text{ and } B = \frac{1}{2}(r_m^2 - r^2). \tag{10}$$

From Eq. (10), the phase can be calculated as

$$\phi_2 = \tan^{-1}\left(-\frac{B}{A}\right) = \cot^{-1}\left[\frac{2rr_m \sin(\phi_{d1} - \phi_{d2})}{(r_m^2 - r^2)}\right]. \tag{11}$$

According to Fresnel equations [10], r can be derived by substituting Eq. (5) into Eq. (11) and expressed as

$$r = \frac{-\cos\phi_1 + \sqrt{\cos^2\phi_1 + \cot^2\phi_2}}{\cot\phi_2} r_m = \frac{n-1}{n+1}, \tag{12}$$

where n is the refractive index of S. Eq. (12) can be rewritten as

$$n = \frac{\cot\phi_2 - r_m\cos\phi_1 + r_m\sqrt{\cos^2\phi_1 + \cot^2\phi_2}}{\cot\phi_2 + r_m\cos\phi_1 - r_m\sqrt{\cos^2\phi_1 + \cot^2\phi_2}}. \tag{13}$$

The camera C with the frame frequency f_c is used to record m frames at time $t_1, t_2, \ldots, t_m$. Each pixel records a series of interference intensities $I_1, I_2, \ldots I_m$, which are the sampled intensities of a sinusoidal signal. The data of ϕ_1 and ϕ_2 can be derived by using the absolute phase determination method [11] and the least-square sinusoidal fitting algorithm [12]. If these processes are applied to all other pixels, then the associated data $\phi_1(x,y)$ and $\phi_2(x,y)$ can be obtained similarly. Substitute them into Eq. (13), the refractive index distribution $n(x,y)$ can be calculated.

In reality, the S is a photoelastic material, its Jones matrix S in Eq. (3) and Eq. (8) should be modified and represented as

$$S = \begin{pmatrix} r_{pp} & r_{ps} \\ r_{sp} & r_{ss} \end{pmatrix}. \tag{14}$$

Consequently, ϕ_1 and ϕ_2 can be derived again with two simultaneous equations Eqs. (3) and (4) and Eqs. (8) and (9), and they can be written as

$$\phi_1 = \tan^{-1}\left[\frac{r_m\cos(\phi_{d1} - \phi_{d2}) + r_{ps}\sin\phi_r}{r_m\sin(\phi_{d1} - \phi_{d2}) - r_{ps}\cos\phi_r}\right], \tag{15}$$

$$\phi_2 = \cot^{-1}\left[\frac{2r_{pp}(r_m\sin(\phi_{d1} - \phi_{d2}) - r_{ps}\cos\phi_r)}{r_m^2 - r_{pp}^2 + r_{ps}^2 - 2r_m r_{ps}\sin(\phi_{d1} - \phi_{d2} - \phi_r)}\right], \tag{16}$$

where $r_{pp} = \frac{(n_e - n_o)\cos 2\alpha + n_e n_o - 1}{(n_e+1)(n_o+1)}$, $r_{ps} = \frac{(n_o - n_e)\sin 2\alpha}{(n_e+1)(n_o+1)}$, n_o is the ordinary refractive index, n_e is the extraordinary refractive index and α is the angle between the principal axis of the stress and the y-axis. Substitute Eq. (15) and Eq. (16) into Eq. (13), the relationship between n and the refractive index variation Δn caused by the residual stress can be obtained, where $\Delta n = n_e - n_o$ is also known as the birefringence. Because a two-dimensional photoelastic model exerted by the forces in its own plane will behave as a general retarder [8], the retardation induced by Δn is proportional to the associated stress variation. Under the experimental conditions $r_m = 99\%$, $\phi_r = 10°$, $\phi_{d1} - \phi_{d2} = 10°$ and $n_o = 1.8$, the relationship between n and Δn can be calculated and depicted in Fig. 2 at $\alpha = 0°$, $30°$, $60°$ or $90°$ by substituting Eqs. (15) and (16) into Eq. (13). From this figure, we can see that the measured data of n is quasi-linear to the stress if $\alpha \neq 90°$. Although the principal axis of the stress at each pixel is different from others, the standard deviation can be measured to show the effect of the residual stress as the resistance measurement in the conventional method.

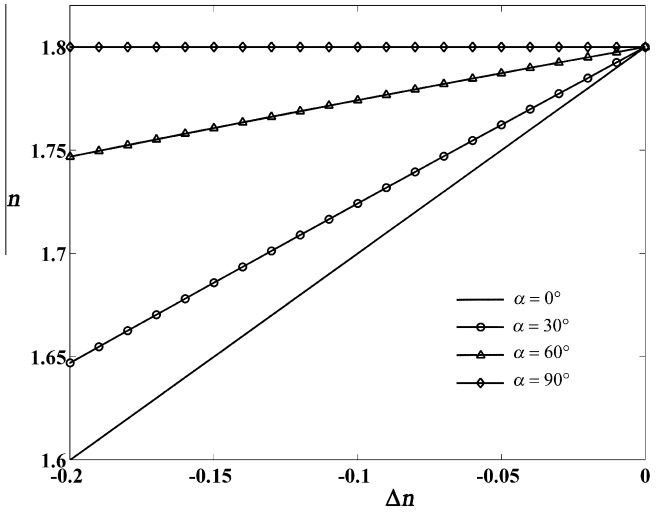

Fig. 2. The relation curves of n versus Δn at different α.

3. Experiments and results

To demonstrate the validity of this technique, an ITO film sample coated on PET layer (CPFilms/OC 100) was tested. The isolation lines with about 0.85 mm pitch were printed on the ITO film with laser patterning processes. It was originally a plane plate as shown in Fig. 3a, where the gray, the white and the black parts represent the ITO film, the PET layer and the isolation lines, respectively. Under the bending test, it was bent with a constant bending force F applied on its two sides simultaneously as shown in Fig. 3b. Then, the bending force was removed and it became a plane plate again. In our tests, it was bent with a bending machine (ITRI-CMS/FCIS/08) under the conditions of 20 mm bending radius, 20°/s bending angular speed, and 8 cycles/min bending frequency. Although it has a 60 mm × 60 mm dimension, only a 260 μm × 260 μm area near its center with higher stress caused by the bending test was measured, as shown in Fig. 3a. An He–Ne laser with 632.8 nm wavelength, an electro-optic modulator (New Focus/Model 4002), a CMOS camera (Basler/A504 K) with 8-bit gray levels and 350 × 350 pixels, a reference mirror with $r_m = 99\%$ and a 10× image lens IL were used. To measure the full-field absolute phase, the saw-tooth voltage signal with the amplitude V being lower than its half-wave voltage V_π was applied to drive the EO, the phase at the break-point position of the periodical sinusoidal segment was used to be the reference phase [11]. Under the conditions $f = 20$ Hz, $V_\pi = 144$ V, $V = 120$ V and $f_c = 300$ frames/s, 300 frames were taken in 1 s each time. For easier reading, the measured results of the two-dimensional refractive index distribution are displayed in color. Fig. 4 shows the results before bending, and Fig. 5a and b show the results after bending 1000 cycles and 4000 cycles, respectively. The mean values of the measured area can be calculated and they are 1.855, 1.849 and 1.811, respectively; that is, they have 0.32% and 2.37% variations. Their associated standard deviations can also be derived and they are 0.006, 0.008, and 0.033, respectively. So, they have 33% and 450% variations.

4. Discussion

For comparison, the resistances of this sample were also measured before/after bend-testing by a digital multimeter (Model 2700, Keithley Instrument Inc.). The nodes are located as shown in Fig. 3a. The measured resistances of the above three situations are 2.613 kΩ, 2.623 kΩ and 2.674 kΩ, respectively. They have 0.38% and 2.33% variations. For easy understanding, the variations

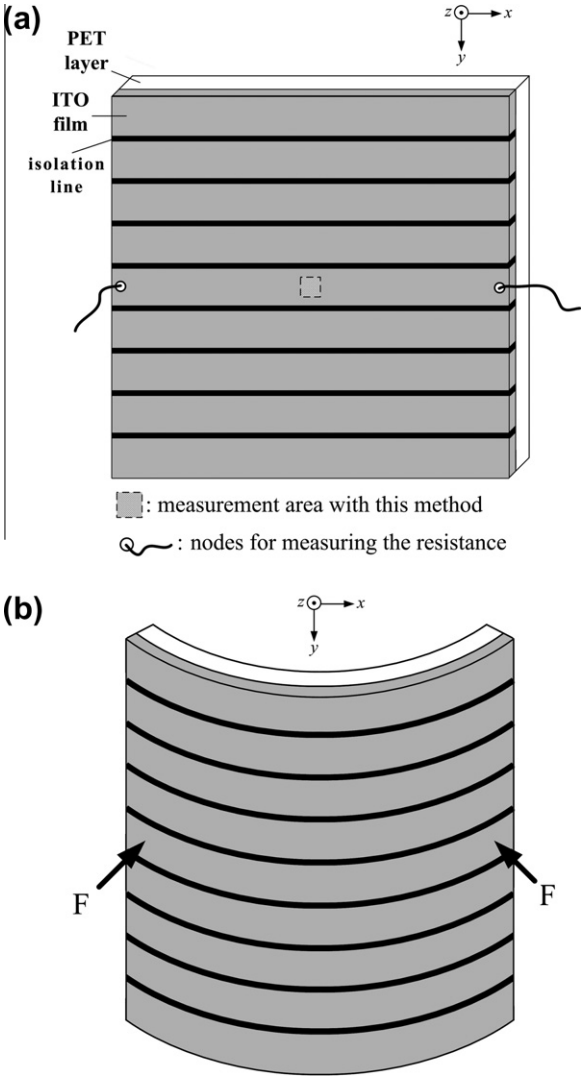

Fig. 3. The sample is (a) unbent and (b) bent; where gray color and white color represent the ITO film and the PET layer, respectively.

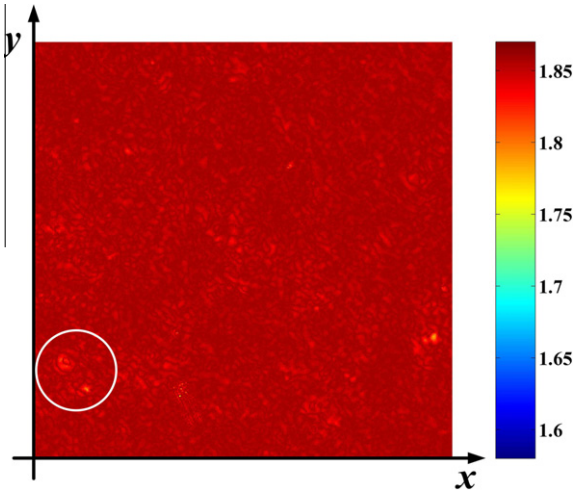

Fig. 4. The two-dimensional refractive index distribution $n(x,y)$ before bending.

of two methods and the standard deviation measured with this method are depicted in Fig. 6. Either the resistance or the mean value of the refractive index acts as an average effect inside the

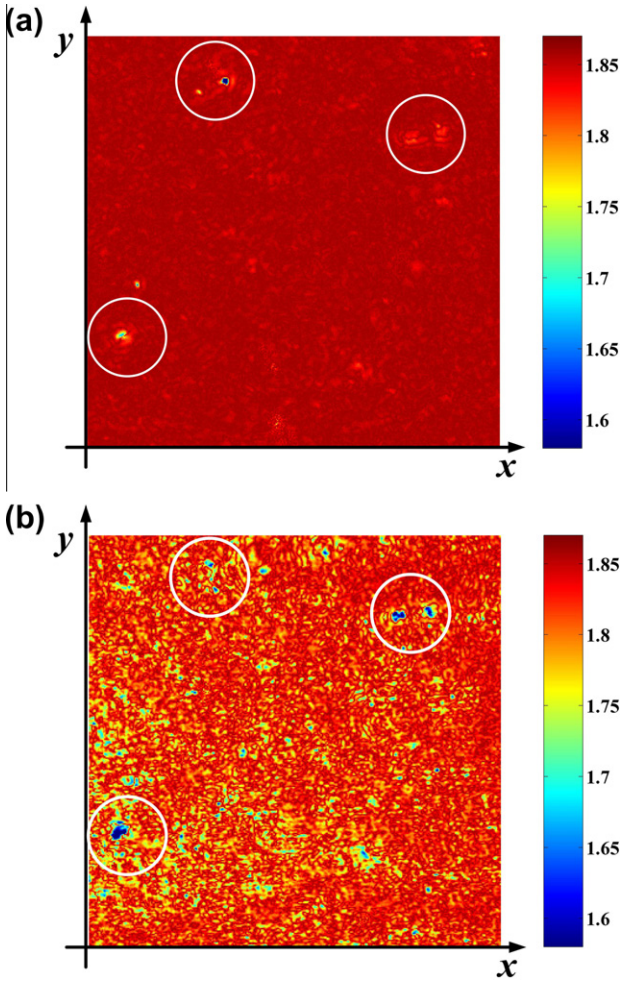

Fig. 5. The two-dimensional refractive index distribution $n(x,y)$ after bending (a) 1000 cycles and (b) 4000 cycles.

conduct area, so they have consistent variations as shown in Fig. 6. From this figure, we can infer that the standard deviation of the refractive index may be used as an indicator to justify the durability of the ITO film. It varies more sensitively than the resistance does.

To collect the reflected parallel beam from the ITO surface and magnify the object simultaneously, it is better to use the imaging lens IL composed of a microscopic objective (MO) and a doublet (DL). Because the IL is an afocal optical system, the ITO surface needs to be located in the front focal plane of the MO and the image plane of the CMOS camera should be correspondingly located in the rear focal plane of the DL. The transverse magnification of the IL in our experiments is −10.

All the lower left circles in Figs. 4, 5a and b have larger refractive index variations, so it has more residual stress. Comparing the data in these three circles, we can see that the residual stress increases with more bending cycles [3–5]. This tendency can be also found in two other circles in Fig. 5a and b.

5. Conclusion

The two-dimensional refractive index distribution of an ITO film deposited on a PET layer has been measured before/after bend-testing with an alternative method based on Fresnel equations and the heterodyne interferometry. The variation of the standard deviation is larger than the resistance variation measured in the

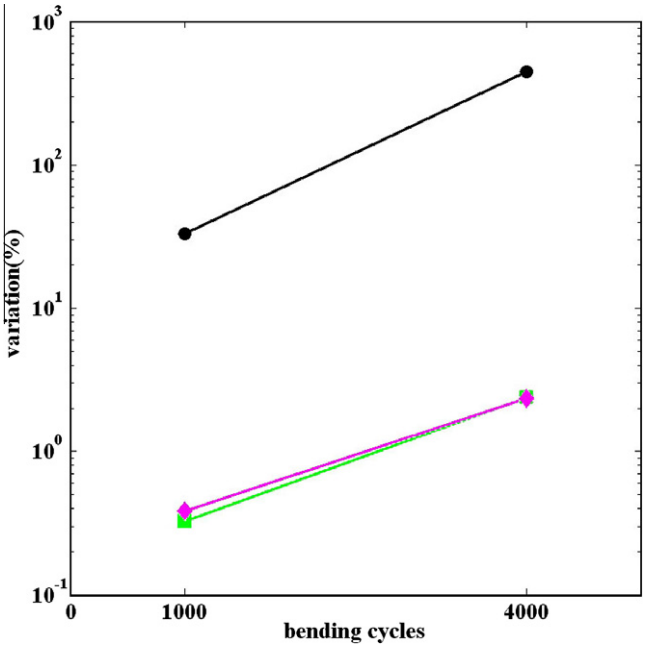

Fig. 6. The variations of the mean value (symbol ■), the standard deviation (symbol ●) of this method, and the resistance (symbol ♦) at 1000 and 4000 bending cycles.

conventional method, so it may be used as the indicator to justify its durability. The validity has been demonstrated.

Acknowledgement

This study was supported in part by the National Science Council, Taiwan, ROC, under Contract NSC95-2221-E009-236-MY3.

References

[1] C. Sujatha, G.M. Rao, S. Uthanna, Characteristics of indium tin oxide films deposited by bias magnetron sputtering, Mater. Sci. Eng. B94 (2002) 106–110.
[2] H.Y. Tsai, H. Yangm, C.T. Pan, M.C. Chou, Laser patterning indium tin oxide (ITO) coated on PET substrate, Proc. SPIE 4230 (2000) 156–163.
[3] S. Grego, J. Lewis, E. Vick, D. Temple, Development and evaluation of bend-testing techniques for flexible-display applications, J. Soc. Inf. Display 13 (2005) 575–581.
[4] S.P. Gorkhali, D.R. Cairns, G.P. Crawford, Reliability of transparent conducting substrates for rollable displays: a cyclic loading investigation, J. Soc. Inf. Display 12 (2004) 45–49.
[5] M.H. Lee, K.Y. Ho, P.C. Chen, C.C. Cheng, S.T. Chang, M. Tang, M.H. Liao, Y.H. Yeh, Promising a-Si:H TFTs with high mechanical reliability for flexible display, Tech. Dig. IEDM (2006) 299–302.
[6] B. J. Wen, T. S. Liu, C. H. Chen, H. Y. Ko, Z. Y. Chung, S. C. Liao, P-72: optical-characteristic measurement of flexible display for reliability test, In: SID Symp. Dig. Tech. Papers, vol. 40, 2009, pp. 1378–1381.
[7] J.R. Lee, D.Y. Lee, D.G. Kim, G.H. Lee, Y.D. Kim, P.K. Song, Characteristics of ITO films deposited on a PET substrate under various deposition conditions, Metal Mater. Int. 14 (2008) 745–751.
[8] K.J. Gåsvik, Optical Metrology, third ed., John Wiley & Sons (2002) 217–245.
[9] D.C. Su, M.H. Chiu, C.D. Chen, Simple two frequency laser, Prec. Eng. 18 (1996) 161–163.
[10] E. Hecht, Optics, forth ed., Addison-Wesley, 2002.
[11] Y.L. Chen, D.C. Su, A method for determining full-field absolute phases in the common-path heterodyne interferometer with an electro-optic modulator, Appl. Opt. 47 (2008) 6518–6523.
[12] IEEE, Standard for Terminology and Test Methods for Analog to-Digital Converters, IEEE Std. 1241–2000 (2000) 25–29.